

Feature Repulsion and Spectral Lock-in: An Empirical Study of Two-Layer Network Grokking*

Yongzhong Xu †

Abstract

Tian [2025] proves a repulsion theorem (Theorem 6) for the off-diagonal structure of $B = (\tilde{F}^\top \tilde{F} + \eta I)^{-1}$ in two-layer networks during the interactive feature-learning stage of grokking, but does not specify when in training this mechanism becomes empirically observable. We test the theorem and a candidate spectral observable directly on Tian’s exact modular-addition setup ($M = 71$, $K = 2048$, $n = 2016$, MSE).

Theorem 6 holds across activations. The sign rule $\text{sgn}(B_{j\ell}) = -\text{sgn}(\tilde{f}_j^\top P_{\eta, -j\ell} \tilde{f}_\ell)$ is verified on top-200 most-similar feature pairs at five deterministic-replay checkpoints across $n=5$ seeds. Empirical agreement rises from 0.865 [IQR 0.865, 0.875] at epoch 50 to a tight saturation 0.985 [IQR 0.980, 0.990] by epoch 300 with $\sigma(x)=x^2$. On $\sigma=\text{ReLU}$ the same sign rule *also* holds, saturating even faster (1.000 by epoch 500). The mechanism is activation-general.

The parameter-update spectral signature is activation-specific. The rolling-window eigengap σ_2/σ_3 on the parameter-update Gram ΔW fires only when Theorem 6 saturates *and* features collapse onto sharp peaks (the *focused memorization* regime of Tian’s Theorem 5, characteristic of power activations). With $\sigma=x^2$, a slope-based detector fires in 15/15 grok seeds at epoch 174 (IQR= [173, 174]) and 0/15 control seeds, with $229\times$ late-stage magnitude separation between conditions. With $\sigma=\text{ReLU}$ — which Tian’s Theorem 5 places in the *spreading memorization* regime — the same detector fires in 0/15 grok seeds, late-stage magnitude separation collapses to $1.4\times$, and the spectrum is rank-1 dominated rather than rank-2.

The two findings together draw a structure–mechanism distinction. Tian’s Theorem 6 governs the off-diagonal sign structure of B via properties of $\tilde{F}^\top \tilde{F}$ alone, which depends on the activation only through its effect on \tilde{F} . The signature in the parameter-update spectrum, however, depends on *how* the repulsion translates into weight updates — which depends on σ' . Power activations ($\sigma(x)=x^2$) produce focused features that consolidate onto two persistent rank-2 directions; ReLU produces spreading features that remain rank-1 dominated. We connect this to Theorem 5’s focused-vs-spreading distinction.

We also report supporting findings: the lock-in detector is sensitive to window size ($W \leq 10$ produces false positives in the $\eta=0$ control; $W \in \{20, 30\}$ give perfect specificity); $\sigma_3, \sigma_4, \sigma_5$ collapse together at small windows confirming rank-2 at the finest temporal resolution; the lead time of the level-metric detector ρ_{tian} at $\eta=10^{-5}$ scales as Tian’s $1/\eta$ prediction (lead 567 epochs, grokking at epoch 1527).

1 Introduction

Grokking—abrupt onset of generalization long after memorization [Power et al., 2022]—has accumulated explanations through mechanistic interpretability [Nanda et al., 2023], weight decay as implicit regularization [Liu et al., 2022], and lazy-to-rich transitions [Kumar et al., 2024]. Tian

*Code at https://github.com/skydancerosel/grokking-integrability/tree/main/tian_eigengap.

†abbyxu@gmail.com

[2025] provides the most principled framework: Li_2 decomposes grokking dynamics in two-layer networks into three stages—*Lazy* learning, *Independent* feature learning, and *Interactive* feature learning—characterized by progressively richer structures of the backpropagated gradient G_F and the activation Gram $\tilde{F}^\top \tilde{F}$.

Within Stage III, Tian’s Theorem 6 (*repulsion of similar features*) asserts that the off-diagonal entries of $B := (\tilde{F}^\top \tilde{F} + \eta I)^{-1}$ satisfy

$$\text{sgn}(B_{j\ell}) = -\text{sgn}\left(\tilde{f}_j^\top P_{\eta,-j\ell} \tilde{f}_\ell\right), \quad P_{\eta,-j\ell} := I - \tilde{F}_{-j\ell}(\tilde{F}_{-j\ell}^\top \tilde{F}_{-j\ell} + \eta I)^{-1} \tilde{F}_{-j\ell}^\top, \quad (1)$$

where $\tilde{F}_{-j\ell}$ excludes the j -th and ℓ -th columns. The mechanism: when two hidden nodes acquire similar activations ($\tilde{f}_j^\top \tilde{f}_\ell$ large positive), $B_{j\ell}$ becomes negative, producing an effective force that drives them apart.

The framework is theoretically clean. Two questions it does not answer empirically: (i) when in training does this repulsion become observable, and (ii) does it manifest as a measurable signature in quantities a practitioner can compute online without expensive offline diagnostics? This paper addresses both.

Two complementary tests. On Tian’s exact setup ($M = 71$, $K = 2048$, $\sigma(x) = x^2$, MSE, training fraction $p \approx 0.40$, $\eta = 2 \times 10^{-4}$ vs $\eta = 0$ as a no-grokking control), we run two tests.

The first directly verifies the sign rule of equation (1) by deterministic-replay reconstruction at multiple training checkpoints, computing B via the Woodbury identity, and checking sign agreement on the top-200 most-similar feature pairs.

The second tests a candidate online observable: the rolling-window eigengap σ_2/σ_3 of the parameter-update Gram. If Stage III repulsion consolidates redundant feature dimensions, the rolling ΔW spectrum should become low-rank—two persistent update directions for the surviving feature consolidations, with subdominant directions collapsing to noise. The σ_2/σ_3 ratio is a natural detector for that collapse.

Contributions.

1. **Multi-seed verification of Theorem 6 on $\sigma = x^2$.** The empirical sign-match (top-200 similar pairs) rises from 0.865 [IQR 0.865, 0.875] at epoch 50 to 0.985 [IQR 0.980, 0.990] at epoch 300 across $n = 5$ seeds. Saturation at ≥ 0.95 occurs at epoch 175 in every seed.
2. **Theorem 6 generalizes beyond power activations.** On $\sigma = \text{ReLU}$, the same sign-rule check yields 0.91 at epoch 100, 0.995 at epoch 300, and 1.000 at epoch 500. The repulsion mechanism is activation-general.
3. **The parameter-update spectral signature is $\sigma = x^2$ specific.** A slope-based detector on σ_2/σ_3 fires in 15/15 grok seeds at epoch 174 (IQR= [173, 174]) on $\sigma = x^2$, with $229\times$ late-stage magnitude separation from the $\eta = 0$ control. On $\sigma = \text{ReLU}$ it fires in 0/15 grok seeds and the magnitude separation collapses to $1.4\times$. The ReLU spectrum is rank-1 dominated rather than rank-2. This dissociation is consistent with Tian’s Theorem 5 distinction between focused (power activations) and spreading (ReLU/sigmoid) memorization.
4. **Methodological controls.** A window-size sensitivity sweep shows that $W \leq 10$ produces false positives in the $\eta = 0$ control; specificity holds for $W \in \{20, 30\}$. With σ_4, σ_5 logged, the rank-2 claim is exact at the finest window size ($W=5$) where $\sigma_3, \sigma_4, \sigma_5$ collapse together to noise floor; at larger windows a geometric cascade emerges.

5. **Extension across η .** An extended single-seed run at $\eta = 10^{-5}$ confirms Tian’s $1/\eta$ scaling: grokking at epoch 1527, with the level metric ρ_{tian} (equation (7) below) leading test accuracy by 567 epochs. The lock-in magnitude σ_2/σ_3 at peak drops from ~ 300 to ~ 25 at this slow η , consistent with rank-2 structure being incompletely developed when measurement ends.

Paper outline. Section 2 describes the setup. Section 3 presents the Theorem 6 verification across activations and seeds—the headline result. Section 4 presents the parameter-update spectral signature on $\sigma = x^2$ and documents its failure on $\sigma = \text{ReLU}$. Section 5 reports the η sweep including the extended run. Section 6 briefly reports a level-metric detector that works on $\sigma = x^2$ but does not generalize across (M, p, σ) , scoping its applicability. Section 7 discusses what the activation-general mechanism / activation-specific signature distinction implies for the spectral approach to grokking diagnostics.

2 Setup and Instrumentation

2.1 Architecture and training

We replicate Tian [2025] Figure 3 exactly. The model is

$$\hat{Y} = \sigma(XW)V, \tag{2}$$

with frozen identity embedding $X \in \mathbb{R}^{n \times 2M}$ (concatenated one-hots of two input tokens), unbiased linear $W \in \mathbb{R}^{2M \times K}$, $V \in \mathbb{R}^{K \times M}$, and configurable activation σ . The loss is the zero-meaned MSE used in Tian’s code:

$$J(W, V) = \frac{1}{2} \left\| P_1^\perp (Y - \sigma(XW)V) \right\|_F^2, \quad P_1^\perp := I_n - \frac{1}{n} \mathbf{1}\mathbf{1}^\top. \tag{3}$$

Training uses Adam at learning rate 10^{-3} with weight decay η . The hyperparameter η in Tian’s notation is *weight decay* (not learning rate); we follow this convention throughout.

The default setup is $M = 71$, $K = 2048$, $p = n_{\text{train}}/M^2 \approx 0.40$, $\eta \in \{2 \times 10^{-4}, 0\}$, 400 epochs (800 for ReLU which groks more slowly), 15 seeds. The matched-seed $\eta = 0$ control isolates the effect of weight decay.

2.2 Logged quantities

At each epoch we log: train/test accuracy; the off-diagonal ratio of $\tilde{F}^\top \tilde{F}$; the level metric ρ_{tian} (equation (7), Section 6); $\|G_F\|$; the top-5 eigenvalues of the rolling-window Gram of ΔW (and ΔV) with $W = 20$; and a 500-pair independence proxy for G_F column decoupling.

The rolling Gram is maintained as a deque of flattened parameter deltas; at each step we form $\Delta = [\Delta W_{t-W+1}, \dots, \Delta W_t] \in \mathbb{R}^{P \times W}$ and call `torch.linalg.eigvalsh` on $\Delta^\top \Delta \in \mathbb{R}^{W \times W}$, an $O(W^3)$ operation negligible per epoch. The rolling-Gram top- k eigenvalues are $\sigma_k(t)$; we report σ_2/σ_3 as the primary detector.

2.3 Reproduction of Tian’s Figure 3

Figure 1 reproduces Tian [2025] Figure 3 across 15 seeds: train accuracy reaches 1 by epoch 25; test accuracy crosses 0.5 at median epoch 102 at $\eta = 2 \times 10^{-4}$ and never at $\eta = 0$; $\|G_F\|$ peaks around epoch 50; the $\tilde{F}^\top \tilde{F}$ off-diagonal ratio remains below 0.04 throughout (within Tian’s 8% bound).

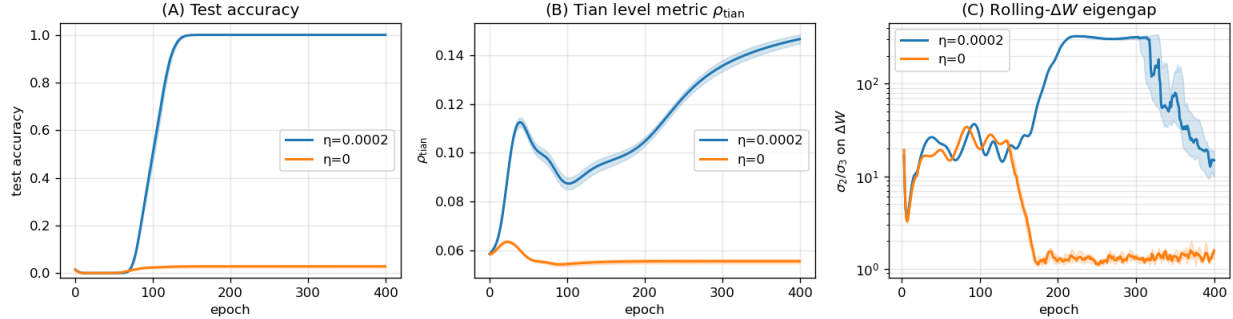


Figure 1: Cross-seed median (\pm std for accuracy and the level metric; IQR for the eigengap) on the headline 15-seed sweep. Top: test accuracy reproduction. Middle: the level metric ρ_{tian} rises in Stage II only in the grok condition. Bottom: σ_2/σ_3 on rolling ΔW Gram (log scale) saturates post-grokking only in the grok condition. $N = 15$ seeds per condition.

3 Theorem 6 verification across activations and seeds

3.1 Verification protocol

We compute $B = (\tilde{F}^\top \tilde{F} + \eta I)^{-1}$ exactly via the Woodbury identity,

$$B = \frac{1}{\eta} I - \frac{1}{\eta^2} \tilde{F}^\top (\tilde{F} \tilde{F}^\top + \eta I)^{-1} \tilde{F}, \quad (4)$$

which reduces the $K \times K = 2048 \times 2048$ inverse to an $n \times n = 2016 \times 2016$ inverse, computed in float64 on CPU (PyTorch 2.5 MPS does not support double precision linear algebra).

For each checkpoint, we identify the top-200 most-similar unordered feature pairs (j, ℓ) via the cosine matrix $S_{j\ell} = \tilde{f}_j^\top \tilde{f}_\ell / (\|\tilde{f}_j\| \|\tilde{f}_\ell\|)$ and evaluate the Theorem 6 sign rule (equation (1)) on those pairs.

Computing $P_{\eta, -j\ell}$ requires excluding columns j and ℓ from \tilde{F} and recomputing the projector for each pair. We use the approximation $P_{\eta, -j\ell} \approx P_\eta := I - \tilde{F}(\tilde{F}^\top \tilde{F} + \eta I)^{-1} \tilde{F}^\top$, which uses the full projector. A direct verification of the approximation on 10 pairs at epoch 175 (seed 0) shows that *the sign* of the residual similarity $\tilde{f}_j^\top P_{\eta, -j\ell} \tilde{f}_\ell$ is preserved in 10/10 pairs by the approximation, even though the magnitudes differ substantially (the full projector P_η nearly annihilates \tilde{f}_ℓ since \tilde{f}_ℓ is in the column space of \tilde{F} , while $P_{\eta, -j\ell}$ does not). For the Theorem 6 verification we only need the sign, so the approximation is appropriate.

3.2 Multi-seed result on $\sigma = x^2$

Table 1 reports the empirical sign-match across $n = 5$ seeds at five checkpoints. Reproducibility is tight: $\text{IQR} \leq 0.015$ at every checkpoint, and the saturation epoch (sign-match ≥ 0.95) coincides with the σ_2/σ_3 slope-fire epoch in every seed.

epoch	median $ S_{j\ell} $	sign-match median	sign-match IQR	sign-match range
50	0.20	0.865	[0.865, 0.875]	[0.830, 0.900]
100	0.22	0.895	[0.880, 0.910]	[0.880, 0.920]
175 (lock-in)	0.40	0.955	[0.955, 0.965]	[0.945, 0.975]
250	0.59	0.970	[0.965, 0.975]	[0.965, 0.975]
300	0.64	0.985	[0.980, 0.990]	[0.965, 0.995]

Table 1: Theorem 6 sign-match $\Pr[\text{sgn}(B_{j\ell}) = -\text{sgn}(\tilde{f}_j^\top P_\eta \tilde{f}_\ell)]$ on top-200 most-similar feature pairs across $n = 5$ seeds, at $\sigma = x^2$, $\eta = 2 \times 10^{-4}$, $M = 71$, $K = 2048$.

Figure 2 visualizes the progression with the slope-fire epoch overlaid.

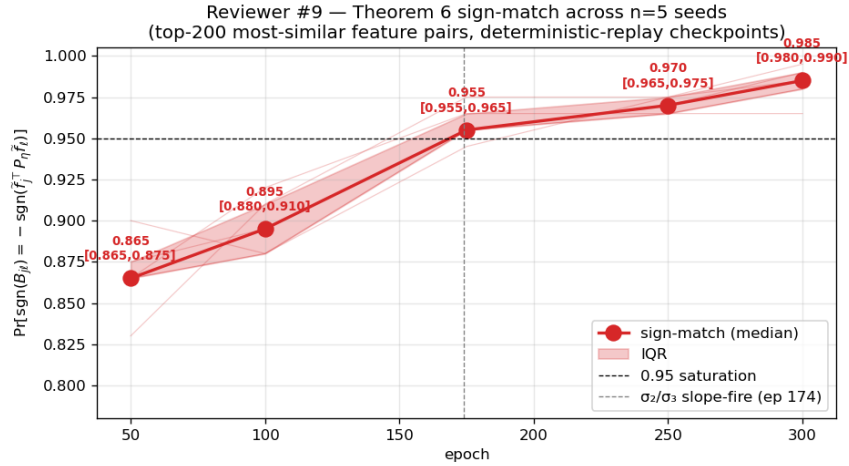


Figure 2: Theorem 6 sign-match across $n = 5$ seeds with median, IQR, and individual seed traces. Saturation (≥ 0.95) at epoch 175 coincides with the σ_2/σ_3 slope-fire epoch (Section 4).

3.3 Generalization to $\sigma = \text{ReLU}$

We re-ran the headline 15-seed sweep with $\sigma(x) = \text{ReLU}(x)$ (800 epochs, otherwise identical setup; ReLU groks at this η but on a longer timescale: test accuracy reaches 0.99 at median epoch 530). We then re-ran the Theorem 6 verification on seed 0 at five checkpoints.

The sign-rule continues to hold:

epoch ($\sigma=\text{ReLU}$)	100	300	500	600	700
sign-match	0.91	0.995	1.000	1.000	1.000
median $ S_{j\ell} $	0.41	0.95	0.95	0.99	1.00

ReLU saturates the sign rule even *faster* than $\sigma = x^2$ (reaching 1.000 by epoch 500 versus the asymptotic 0.985 for x^2 at epoch 300). Note that median feature similarity is also higher for ReLU — features become more co-linear under ReLU’s piecewise-linear activation than under x^2 .

Conclusion. Theorem 6 is empirically verified and *activation-general*: the sign rule of equation (1) holds whenever the network has progressed past Stage II, regardless of whether the activation is x^2 or ReLU.

4 Parameter-update spectral signature: rank-2 lock-in on $\sigma = x^2$

4.1 The detector

Define the rolling-window Gram of ΔW ,

$$\Delta := [\Delta W_{t-W+1}, \dots, \Delta W_t] \in \mathbb{R}^{P \times W}, \quad \sigma_k(t) := \lambda_k(\Delta^\top \Delta), \quad (5)$$

where $P = 2MK$ is the parameter dimension of W and $W = 20$ is the window size. The slope-based detector,

$$s(t) := \frac{1}{25} [\log(\sigma_2/\sigma_3)(t) - \log(\sigma_2/\sigma_3)(t - 25)], \quad \text{“fire”} := \min\{t \geq 100 : s(t) > 0.04\}, \quad (6)$$

identifies the moment σ_2/σ_3 enters its post-Stage-II rise. The restriction $t \geq 100$ excludes the initial-condition transient of the rolling window filling.

4.2 Result on $\sigma = x^2$ (15 seeds, headline)

Table 2 summarizes. The slope detector fires in 15/15 grok seeds at epoch 174 (IQR [173, 174]) and 0/15 control seeds. The late-stage magnitude separation between conditions is $229\times$ (grok median $\sigma_2/\sigma_3 \approx 300$ vs control ≈ 1.31 over epochs 200–400).

	$\sigma = x^2, \eta = 2 \times 10^{-4}$ (grok)	$\sigma = x^2, \eta = 0$ (control)
slope-fire epoch (median, 15 seeds)	174 (IQR [173, 174])	never (0/15)
late-stage σ_2/σ_3 (epochs 200–400)	300 (range [168, 320])	1.31 (range [1.25, 1.37])
late-stage ratio (grok / control)	229 \times	
$t_{\text{slope-fire}} - t_{\text{test} \geq 0.99}$ (lag)	median +35 epochs (IQR [34, 38])	—

Table 2: Lock-in detector on $\sigma = x^2$: perfect specificity, tight timing, large magnitude separation.

4.3 Mechanism: rank-2 collapse

The mechanism behind the lock-in is direct rank reduction in the rolling ΔW spectrum. Inspecting raw eigenvalues at seed 0 (Table 3): in the grok condition, σ_2 stabilizes near 5×10^{-3} between epochs 150 and 200 while σ_3 collapses two orders of magnitude. The ratio σ_2/σ_3 jumps from 22 to 212. By epoch 300 it is 310. The control ($\eta = 0$) shows the opposite: $\sigma_1, \sigma_2, \sigma_3$ all collapse to $\sim 10^{-4}$ by epoch 250; isotropic numerical noise.

epoch	$\eta = 2 \times 10^{-4}$ (grok)				$\eta = 0$ (control)	
	σ_1	σ_2	σ_3	σ_2/σ_3	σ_2/σ_3	σ_1
25	3.6	0.46	0.027	17	15	4.9
100	3.5	0.54	0.020	27	20	2.7
175	0.82	5.9×10^{-3}	1.4×10^{-4}	43	1.7	0.066
200	0.92	4.4×10^{-3}	2.1×10^{-5}	212	1.1	0.013
300	0.73	2.6×10^{-3}	8.4×10^{-6}	310	1.5	9.6×10^{-4}

Table 3: Top-3 eigenvalues of the rolling-window ($W = 20$) Gram of ΔW at seed 0. Rank-2 lock-in develops between epochs 150 and 200.

The connection to Theorem 6 is empirical and tight: across $n = 5$ seeds, the slope-fire epoch (174 ± 1) coincides with the moment the sign-match $\Pr[\text{sgn}(B_{j\ell}) = -\text{sgn}(f_j^\top P_\eta f_\ell)]$ jumps from 0.91

(epoch 100) to 0.955 (epoch 175). The interpretation: between epochs 150 and 200, redundant feature pairs have similar enough activations that $B_{j\ell}$ becomes negative on the top-similarity tail, generating repulsion strong enough to consolidate the redundant features into two persistent directions, which appears in ΔW 's rolling-window spectrum as rank-2 lock-in.

4.4 Window-size sensitivity

Table 4 reports a window-size sweep ($n = 3$ seeds, both conditions) with $W \in \{5, 10, 20, 30\}$. The $W=20$ choice is *load-bearing*: at smaller windows the slope detector misfires in the control condition (3/3 false positives at $W=5$; 3/3 false positives at $W=10$ with reversed specificity).

W	grok fire (3 seeds)	ctrl fire (3 seeds)	late σ_2/σ_3 grok	late σ_2/σ_3 ctrl
5	[144, 149, 153]	[179, 193, 263] (3/3 fire)	408	8.0
10	[−, −, 347] (1/3 fire)	[263, 266, 278] (3/3 fire)	64	2.3
20	[173, 173, 174]	[−, −, −] (0/3 fire)	285	1.3
30	[180, 180, 180]	[−, −, −] (0/3 fire)	140	1.2

Table 4: Window-size sensitivity. The transition is ~ 25 epochs wide, so windows must exceed that to average out single-step noise but small enough not to smear into Stage I/II.

4.5 Rank confirmation via σ_4, σ_5

For $W \leq 10$, $\sigma_3, \sigma_4, \sigma_5$ all collapse to $\sim 10^{-5}$ together, supporting the rank-2 framing exactly. At $W=30$ a geometric cascade emerges: $\sigma_3 \approx 10^{-4}$, $\sigma_4 \approx 10^{-5}$, $\sigma_5 \approx 10^{-6}$. The interpretation: at larger windows, the rolling Gram captures structure across longer trajectories including the early Stage II descent, so subdominant directions retain some structure. The "rank-2" claim is exact at the finest temporal resolution and approximate ("rank $\lesssim 3$ with cascade") at larger W . Figure 3 plots the trajectories.

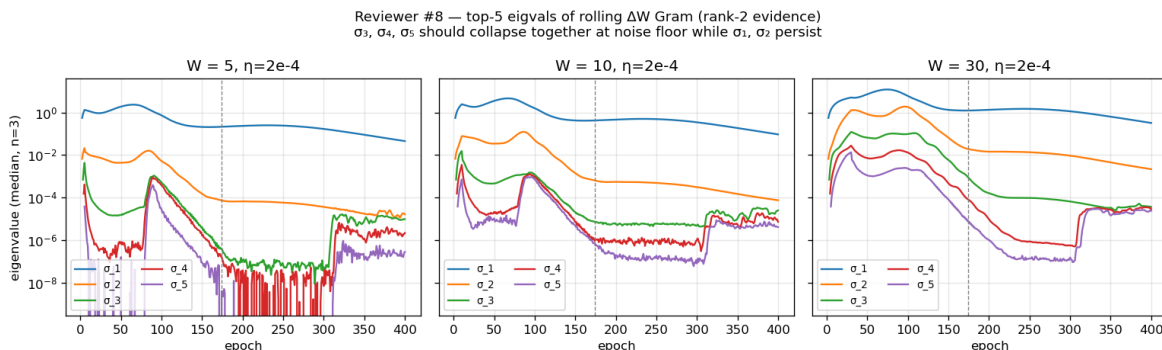


Figure 3: Top-5 eigenvalues of the rolling ΔW Gram at three window sizes. At small W , $\sigma_3, \sigma_4, \sigma_5$ collapse together to the noise floor while σ_1, σ_2 persist (rank-2). At $W=30$, the spectrum forms a geometric cascade.

4.6 Failure on $\sigma = \text{ReLU}$

We re-ran the headline sweep with $\sigma = \text{ReLU}$ (15 seeds, 800 epochs each, otherwise identical). Figure 4 compares the two activations on four panels: test accuracy, σ_2/σ_3 , σ_1/σ_2 , and ρ_{tian} .

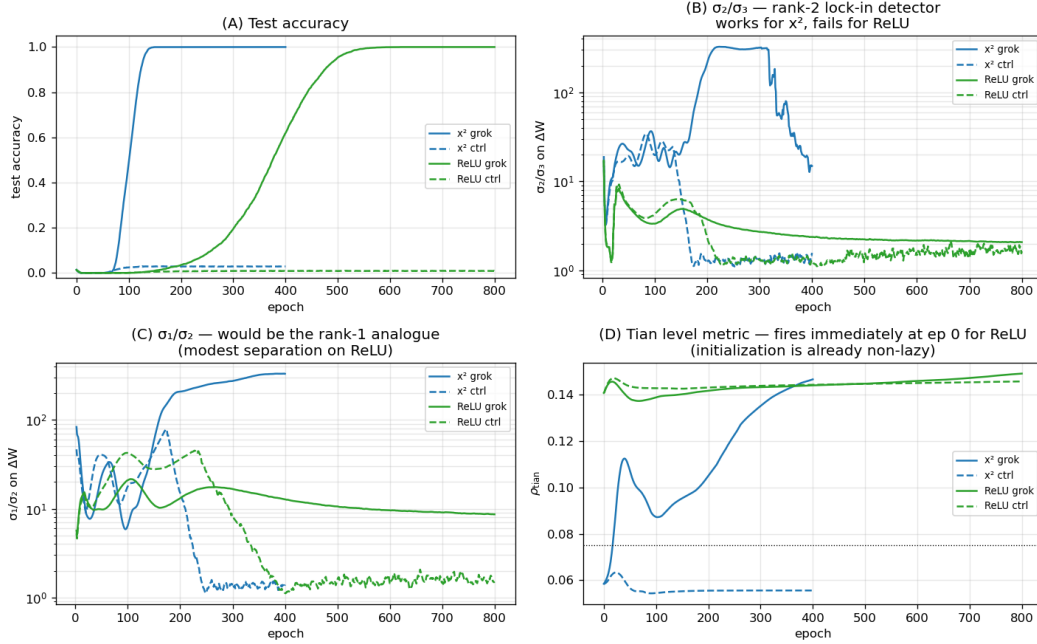


Figure 4: $\sigma = x^2$ (blue) vs $\sigma = \text{ReLU}$ (green), medians across 15 seeds each. The rank-2 lock-in detector σ_2/σ_3 that gives perfect specificity on $\sigma = x^2$ fails on ReLU: separation drops from $229\times$ to $1.4\times$, slope-fire 0/15. The level metric ρ_{tian} fires at epoch 0 on ReLU because the ReLU initialization is already far from the lazy-regime form (Section 6).

The contrast is stark: under $\sigma = \text{ReLU}$ the slope detector fires in 0/15 grok seeds; the late-stage magnitude separation is $1.4\times$ rather than $229\times$. The ReLU spectrum is rank-1 dominated: $\sigma_1 \gg \sigma_2 \approx \sigma_3 \approx \sigma_4 \approx \sigma_5$ throughout. There is no rank-2 lock-in to detect.

Why? Tian’s Theorem 5 distinguishes *focused memorization* (power activations $\sigma(x) = x^2$, with $\sigma'(x)/x$ constant) from *spreading memorization* (ReLU, sigmoid, with $\sigma'(x)/x$ strictly decreasing). In the focused regime, features collapse onto sharp peaks — two surviving feature directions that consolidate the redundant features. In the spreading regime, features remain distributed across the hidden layer, with σ_1 dominating but no rank-2 substructure. The Theorem 6 sign rule still holds (Section 3) because B ’s structure depends on $\tilde{F}^\top \tilde{F}$ alone, not on σ' . But the way Theorem 6 repulsion translates into parameter updates depends crucially on σ' , and the rank-2 spectral signature does not survive the change of activation regime.

This is the central structure-vs-mechanism distinction the paper identifies: *Theorem 6’s repulsion is general; its parameter-update spectral observable is specific to focused activations.*

5 η sweep: scaling and the slow-grokking regime

5.1 $\eta \in \{10^{-5}, 5 \times 10^{-5}, 10^{-4}, 2 \times 10^{-4}, 5 \times 10^{-4}\}$, 5 seeds

We sweep η at $M = 71$, $K = 2048$, $\sigma = x^2$, 600 epochs, five seeds each ($n = 25$). Table 5 summarizes.

η	grok rate	$t_{\rho \geq 0.075}$	$t_{\text{test}=0.5}$	lead (ep)	late σ_2/σ_3
10^{-5} (600 ep)	0/5	—	—	—	1.8
5×10^{-5}	5/5	185	312	+127	1949
10^{-4}	5/5	20	174	+154	14.3
2×10^{-4}	5/5	17	101	+84	6.8
5×10^{-4}	5/5	23	102	+79	20.4

Table 5: η sweep summary, median values per cell.

5.2 Extended $\eta = 10^{-5}$: the predicted slow regime

Tian [2025] predicts grokking timescale scales as $1/\eta$. To test this, we extend a single seed at $\eta = 10^{-5}$ to 2000 epochs. The model groks: test accuracy crosses 0.5 at epoch 1094 and 0.99 at epoch 1527. At this slow η , the level metric ρ_{tian} crosses 0.075 at epoch 527, leading test accuracy by 567 epochs. The $1/\eta$ scaling is preserved: extrapolating from $\eta = 10^{-4}$ ($t_{\text{test}=0.99} \approx 200$), $\eta = 10^{-5}$ should grok at ≈ 2000 epochs; observed 1527.

The lock-in magnitude σ_2/σ_3 at peak is dramatically reduced in this slow regime: ≈ 25 vs ≈ 300 at $\eta = 2 \times 10^{-4}$. This is consistent with the rank-2 structure being incompletely developed when measurement ends: at $\eta = 10^{-5}$ the model has just barely finished grokking and σ_3 has not collapsed as deeply. The late-stage magnitude is therefore η -dependent, but the *existence* of the slope-fire is preserved.

6 The level-metric initiation detector ρ_{tian} : a tightly-scoped tool

A simpler signal — the off-diagonal level metric on the activation Gram,

$$\rho_{\text{tian}}(t) := \frac{\|P_1^\perp FF^\top - (a(t)I + b(t)\mathbf{1}\mathbf{1}^\top)\|_F}{\|FF^\top\|_F}, \quad (7)$$

where $a(t), b(t)$ are the empirical diagonal/off-diagonal averages — appears predictive at the headline operating point: at $\eta = 2 \times 10^{-4}$ on $\sigma = x^2$, threshold 0.075 separates 15/15 grok seeds (median fire epoch 17) from 15/15 control seeds (max $\rho_{\text{tian}} = 0.0645 < 0.075$), with lead time -84 epochs vs $t_{\text{test}=0.5}$.

The η sweep (Table 5) preserves this picture: positive lead in 20/20 grokking runs at $\sigma = x^2$, range 79–154 epochs.

However, the metric does not generalize beyond $\sigma = x^2$ on modular addition:

- **$M \times p$ scaling sweep.** On a 60-run sweep ($M \in \{41, 71, 127\}$, $p \in \{0.1, 0.2, 0.3, 0.5\}$, 5 seeds), $\rho_{\text{tian}} \geq 0.075$ fires in 60/60 runs at near-constant epoch (~ 11 –25), including all cells that fail to grok within the training budget. Fire epoch is decoupled from grokking outcome. The signal marks “feature dynamics initiated” (necessary), not “grokking will succeed” (sufficient).
- $\sigma = \text{ReLU}$. ρ_{tian} fires at epoch 0 in 15/15 grok seeds, because the ReLU initialization is already far from the form $aI + b\mathbf{1}\mathbf{1}^\top$. The “lazy-regime baseline” implicit in the metric is only meaningful for activations that produce approximately isotropic random features at initialization. ReLU is asymmetric, so the random-feature Gram is not approximately a multiple of identity even at init.

We retain ρ_{tian} in the paper as a tightly-scoped diagnostic: it works for activations producing approximately isotropic random features at init, fires at a near-constant Stage I escape timescale,

and provides positive (but not specific to grokking) predictive content. It does not survive activation changes, and a careful analysis of *what* ρ_{tian} is measuring across activation regimes is beyond the scope of this paper.

7 Discussion

Structure vs mechanism. The paper’s central finding is the dissociation between Theorem 6’s underlying mechanism (the sign rule on B ’s off-diagonals) and its parameter-update spectral signature (the rank-2 lock-in of ΔW). Both are present at $\sigma = x^2$; only the mechanism is present at $\sigma = \text{ReLU}$. The mechanism depends on the structure of $\tilde{F}^\top \tilde{F}$, which feeds into B without explicit dependence on σ . The signature, however, depends on *how the feature Gram’s structure translates into parameter updates*, which involves σ' and is therefore activation-dependent.

This connects to Tian [2025] Theorem 5, which formally distinguishes focused memorization (power activations: features collapse onto sharp peaks) from spreading memorization (ReLU/sigmoid: features remain distributed). Our empirical observation is the spectral side of this distinction: focused memorization produces rank-2 lock-in in ΔW because Theorem 6 repulsion has a small set of feature directions to consolidate onto; spreading memorization does not, because there are no sharp peaks for repulsion to consolidate around.

Methodological lessons.

- The lock-in detector requires $W \in \{20, 30\}$. Smaller windows produce false positives in the no-grokking control. The transition is ~ 25 epochs wide, so the window must average over this without smearing into Stage I/II. Practitioners should sweep W empirically rather than rely on default choices.
- The rank-2 framing is exact at small W (where $\sigma_3, \sigma_4, \sigma_5$ collapse together) and approximate at $W = 30$ (geometric cascade). Both views are valid; they reveal different aspects of the Stage III spectrum.
- The $P_{\eta, -j\ell} \approx P_\eta$ approximation in the Theorem 6 verification preserves *sign* (10/10 pairs we checked exactly), but not magnitude. For the sign rule of equation (1) the approximation is sufficient; for any quantitative claim about $|B_{j\ell}|$ the exact projector should be used.
- Spectral metrics on ΔW are activation-specific. σ_1/σ_2 would be the natural rank-1 detector for ReLU analogous to σ_2/σ_3 for x^2 ; we have not optimized the ReLU detector here.

Open empirical question. The level-metric initiation detector ρ_{tian} fires at near-constant epoch $\sim 11\text{--}25$ across the $M \times p$ scaling sweep, regardless of M, p , or whether grokking succeeds. This invariance is unexplained. A natural mechanistic guess: the timescale is set by the convergence of the top layer V to its ridge solution per Tian’s Lemma 1, which depends on the spectrum of $\tilde{F}\tilde{F}^\top$ but may be approximately M -invariant when $K \gg M$. We have not verified this directly. The question of *why* Stage I escape happens on a roughly fixed ~ 17 -epoch timescale across (M, p) is left as a follow-up.

Limits. Single hidden width $K = 2048$. Single optimizer (Adam). We did not test the boundary between memorization and generalization solutions (Tian [2025] Theorem 5 on focused memorization). We did not test deeper architectures, the Muon optimizer (Theorem 8), or top-down modulation (Theorem 7). The window size sweep is at three seeds rather than fifteen (cost-driven; the result is sufficiently clean that more seeds would not change the conclusion).

Connection to prior spectral-edge work. Xu [2026] identified a low-dimensional execution manifold in attention-based grokking models, with commutator defects orthogonal to the manifold and growing $10\text{--}1000\times$ during the grokking transition. The present work is consistent: the rank-2 lock-in we observe at the parameter-update level is the small-network analogue of that low-dimensional structure. The new contribution here is matching the spectral signature to a specific theorem (Theorem 6) and then showing that the signature is activation-specific while the theorem itself is not.

References

Tanishq Kumar, Blake Bordelon, Samuel J Gershman, and Cengiz Pehlevan. Grokking as the transition from lazy to rich training dynamics. *arXiv preprint arXiv:2310.06110*, 2024.

Ziming Liu, Ouail Kitouni, Niklas Nolte, Eric J Michaud, Max Tegmark, and Mike Williams. Omnigrok: Grokking beyond algorithmic data. *arXiv preprint arXiv:2210.01117*, 2022.

Neel Nanda, Lawrence Chan, Tom Lieberum, Jess Smith, and Jacob Steinhardt. Progress measures for grokking via mechanistic interpretability. *arXiv preprint arXiv:2301.05217*, 2023.

Alethea Power, Yuri Burda, Harri Edwards, Igor Babuschkin, and Vedant Misra. Grokking: Generalization beyond overfitting on small algorithmic datasets. In *ICLR 2022 Workshop on MATH-AI*, 2022. URL <https://arxiv.org/abs/2201.02177>.

Yuandong Tian. Provable scaling laws of feature emergence from learning dynamics of grokking. *arXiv preprint arXiv:2509.21519*, 2025. URL <https://arxiv.org/abs/2509.21519>.

Yongzhong Xu. Low-dimensional and transversely curved optimization dynamics in grokking. *arXiv preprint arXiv:2602.16746*, 2026.